Ground-source pump system for heating and cooling: Review and thermodynamic approach

Communication

On the Computation of Square Roots and Inverse Square Roots of Gram Matrices for Surface Integral Equations in Electromagnetics

Rui Chen, Adrien Merlini, and Francesco P. Andriulli

***Abstract*—Surface integral equations (SIEs) are widely used for modeling electromagnetic scattering problems. However, after their discretization via the boundary element method (BEM), the spectra and eigenvectors of resulting matrices are not usually representative of those of underlying surface integral operators, which can be problematic for methods that rely heavily on spectral properties. To address this issue, the spectrum of the integral operators can be recovered, while preserving symmetry, using square roots and inverse square roots of Gram matrices. In this work, several algorithms are delineated for the computation of square roots and inverse square roots of several relevant Gram matrices. The algorithms we detail rely on properly chosen polynomial expansions of the scalar square root and inverse square root functions and the theory of matrix functions. Tables containing different sets of expansion coefficients are provided along with comparative numerical experiments that evidence the advantages and disadvantages of the different approaches. In addition, the use of the proposed techniques as a tool for the recovery of the spectrum of integral operators is illustrated in the case of a spherical geometry for which the analytic spectrum is known.**

***Index Terms*—Gram matrix, matrix function, polynomial expansion, spectral analysis, surface integral equation (SIE).**

I. Introduction

The boundary element method (BEM) is widely used for analyzing electromagnetic scattering from perfectly electrically conducting (PEC) objects. For such scatterers, the BEM is typically used to discretize surface integral equations (SIEs), such as the electric field integral equation (EFIE), the magnetic field integral equation, and their linear combinations. Different from differential equation (DE)-based methods, the BEM does not require the use of artificial absorbing boundary conditions for truncating the physical domain into a finite computational domain. Moreover, the BEM requires only the surface of the scatterer to be discretized, using boundary elements, which results in comparatively fewer unknowns compared to the DE-based methods [1].

To numerically solve SIEs, surface integral operators are discretized by expanding the surface current with basis functions and testing the resulting equation, which yields a matrix system. Then, direct solvers or iterative solvers coupled with fast matrix-vector product algorithms are used to solve the system for the current expansion coefficients.

However, the spectrum and eigenvectors of the resulting boundary element matrices are not usually representative of those of the underlying surface integral operators. It is partly because, in general, the boundary elements do not form an orthonormal basis of the spaces they span and the operators' eigenvalues can be recovered through a generalized eigenvalue problem [2]. While it is not necessarily problematic for standard solution strategies, some numerical methods rely on delicate spectral manipulations that necessitate the correspondence between the spectra of the operator to be discretized and that of the corresponding boundary element matrix [3]. To solve this issue, one could use orthonormal basis functions, but they are often impractical.

Other approaches leveraging the Gram matrices [4] of the bases used in the discretization of the integral operators have been proposed. For instance, when the symmetry of the original problem does not need to be maintained, the multiplication by the inverse of the Gram matrices [5] can be used to reconstruct the operator spectrum. Instead, when the symmetry must be preserved, an a posteriori orthonormalization of the bases using square roots and inverse square roots of these Gram matrices—as delineated, for instance, in [3] and references therein—can be used. To compute the square roots and inverse square roots of the Gram matrices, the singular value decomposition (SVD) [4] could be used. However, because of its prohibitive computational cost, SVD quickly becomes impractical for large problems. Alternatively, several algorithms have been presented to compute these matrices—such as the Schur method [6], the Newton method [7], or the matrix sign function [8] to name a few—and their theory is well-established. Nonetheless, the application of these schemes to the variety of the Gram matrices appearing in the integral equations-relevant scenarios is not trivial. A specific set of approaches must be selected among many and the associated parameters need to be optimized to avoid instability issues [7] and ensure a computational complexity compatible with traditional fast solution and iterative eigenproblem methods [9].

In this work, several strategies inherited from scalar polynomial expansion approaches are delineated and tailored for the evaluation of the square roots and inverse square roots of several of the most relevant Gram matrices for SIEs in electromagnetics. To numerically compute these matrices suitably chosen polynomial expansions of

Received 28 July 2024; revised 3 March 2025; accepted 17 April 2025. Date of publication 14 May 2025; date of current version 6 August 2025. This work was supported in part by the National Natural Science Foundation of China (NSFC) under Grant 62201264 and Grant 62331016; in part by the Fundamental Research Funds for the Central Universities under Grant 30924010207; in part by the Fund Program for the Scientific Activities of Selected Returned Overseas Professionals in Shanxi Province under Grant 20240063; in part by the Foundation of Anhui Key Laboratory of Industrial Energy-Saving and Safety under Grant KFKT202306; in part by European Innovation Council (EIC) through European Union's Horizon Europe Research Programme (Project CEREBRO) under Grant 101046748; in part by European Union–Next Generation EU within the PNRR Project "Multiscale Modeling and Engineering Applications" of Italian National Center for High-Performance Computing (HPC), Big Data and Quantum Computing (Spoke 6)–PNRR M4C2, Investimento 1.4–Avviso n. 3138 del 16/12/2021–CN00000013 National Centre for HPC, Big Data and Quantum Computing (HPC) under Grant CUP E13C22000990001; and in part by the Labex CominLabs Excellence Laboratory under the National Research Agency in the "Investing for the Future" Program through French Government (Project "CYCLE") under Grant ANR-10-LABX-07-01. *(Corresponding author: Rui Chen.)*

Rui Chen was with the Department of Electronics and Telecommunications, Politecnico di Torino, 10129 Turin, Italy. He is now with the School of Microelectronics, Nanjing University of Science and Technology, Nanjing 210094, China, and also with North Automatic Control Technology Institute, Taiyuan 030006, China (e-mail: rui.chen@njust.edu.cn).

Adrien Merlini is with the Department of Microwave, IMT Atlantique, 29238 Brest, France (e-mail: adrien.merlini@imt-atlantique.fr).

Francesco P. Andriulli is with the Department of Electronics and Telecommunications, Politecnico di Torino, 10129 Turin, Italy (e-mail: francesco.andriulli@polito.it).

Digital Object Identifier 10.1109/TAP.2025.3568083

the scalar square root and inverse square root functions are used in conjunction with the theory of matrix functions [10]. Note that the techniques delineated here could also be used in applications beyond electromagnetics in which Gram matrices are useful, for instance, in quantum mechanics and quantum theory [11]. Tables containing expansion coefficients are provided along with numerical experiments that illustrate the merits and the shortcomings of the different approaches along with a thorough performance analysis. To demonstrate the applicability of the proposed techniques, numerical examples showing how the spectrum of the integral operators can be recovered from a standard boundary element matrix are presented for the scattering from a PEC sphere for which the analytic spectrum is known. A preliminary version of this communication with limited implementation details was presented in [12].

II. Background

Let S denote the surface of a PEC scatterer residing in an unbounded homogeneous background medium with permittivity ε and permeability μ. The PEC scatterer is excited by an electromagnetic wave with the incident electric field $\mathbf{E}^{\text{inc}}(\mathbf{r})$. Upon excitation, the surface current $\mathbf{J}(\mathbf{r})$ induced on S generates the scattered electric field $\mathbf{E}^{\text{sca}}(\mathbf{r})$ in the background medium. The total electric field $\mathbf{E}^{\text{tot}}(\mathbf{r}) = \mathbf{E}^{\text{inc}}(\mathbf{r}) + \mathbf{E}^{\text{sca}}(\mathbf{r})$ satisfies the boundary condition $\hat{\mathbf{n}}(\mathbf{r}) \times \mathbf{E}^{\text{tot}}(\mathbf{r}) = 0$ for $\mathbf{r} \in S$ from which EFIE is expressed as

$$-\hat{\mathbf{n}}(\mathbf{r}) \times \mathbf{E}^{\text{inc}}(\mathbf{r}) = \mathcal{T}[\mathbf{J}](\mathbf{r}) = \hat{\mathbf{n}}(\mathbf{r}) \times \left\{ -j\omega\mu \int_S g(\mathbf{r},\mathbf{r}')\mathbf{J}(\mathbf{r}')ds' - \frac{j}{\omega\varepsilon}\nabla \int_S g(\mathbf{r},\mathbf{r}')\nabla'_s \cdot \mathbf{J}(\mathbf{r}')ds' \right\}. \quad (1)$$

Here, $\hat{\mathbf{n}}(\mathbf{r})$ is the outward pointing unit normal vector, $g(\mathbf{r},\mathbf{r}') = e^{-jkR}/(4\pi R)$ is the Green function, $k = \omega\sqrt{\mu\varepsilon}$ is the wavenumber, and $R = |\mathbf{r}-\mathbf{r}'|$ represents the distance between the field and source points. Note that, the time-harmonic factor $e^{j\omega t}$ is assumed and suppressed throughout this work.

To numerically solve (1) for $\mathbf{J}(\mathbf{r})$, S is meshed using triangular patches. Then, $\mathbf{J}(\mathbf{r})$ is expanded using Rao-Wilton-Glisson (RWG) basis functions [13] as $\mathbf{J}(\mathbf{r}) = \sum_{n=1}^{N_{\text{E}}} \{\mathbf{j}\}_n \mathbf{f}_n(\mathbf{r})$. Here, N_{E} denotes the number of edges of the mesh, $\mathbf{j}$ is the vector containing the N_{E} expansion coefficients to be solved for, and the nth RWG basis function $\mathbf{f}_n(\mathbf{r})$ is defined as $\mathbf{f}_n(\mathbf{r}) = (\mathbf{r} - \mathbf{r}_n^+)/(2A_n^+)$ if $\mathbf{r} \in t_n^+$ and $\mathbf{f}_n(\mathbf{r}) = (\mathbf{r}_n^- - \mathbf{r})/(2A_n^-)$ if $\mathbf{r} \in t_n^-$, where t_n^+ and t_n^- are two triangular patches sharing the nth edge, $\mathbf{r}_n^+$ and $\mathbf{r}_n^-$ are the vertices of t_n^+ and t_n^- that do not belong to the nth edge, and A_n^+ and A_n^- are the areas of t_n^+ and t_n^-, respectively.

Next, rotated RWG functions $\hat{\mathbf{n}}(\mathbf{r}) \times \mathbf{f}_m(\mathbf{r})$, $m = 1, 2, \ldots, N_{\text{E}}$, are used to test the equation yielding a fully discretized matrix equation

$$\mathbf{T}\mathbf{j} = \mathbf{v}. \quad (2)$$

Here, the entries of the boundary element matrix $\mathbf{T}$ has dimension $N_{\text{E}} \times N_{\text{E}}$ and the right-hand side vector $\mathbf{v}$ has N_{E} elements. Their elements are $\{\mathbf{T}\}_{mn} = \langle \hat{\mathbf{n}}(\mathbf{r}) \times \mathbf{f}_m(\mathbf{r}), \mathcal{T}[\mathbf{f}_n](\mathbf{r}) \rangle$, and $\{\mathbf{v}\}_m = -\langle \hat{\mathbf{n}}(\mathbf{r}) \times \mathbf{f}_m(\mathbf{r}), \hat{\mathbf{n}}(\mathbf{r}) \times \mathbf{E}^{\text{inc}}(\mathbf{r}) \rangle$, respectively, where $\langle \cdot, \cdot \rangle$ denotes the appropriate bilinear form and, which for all cases studied in the communication, can be computed as $\langle \mathbf{a}(\mathbf{r}), \mathbf{b}(\mathbf{r}) \rangle = \int_{S_{\text{a}}} \mathbf{a}(\mathbf{r}) \cdot \mathbf{b}(\mathbf{r}) ds$ for vector functions, $\langle a(\mathbf{r}), b(\mathbf{r}) \rangle = \int_{S_{\text{a}}} a(\mathbf{r}) b(\mathbf{r}) ds$ for scalar functions, and S_{a} is the support of $\mathbf{a}(\mathbf{r})$ or $a(\mathbf{r})$.

For certain applications, such as preconditioning [14], the electric field integral operator (EFIO) $\mathcal{T}$ must also be discretized using Buffa-Christiansen (BC) basis functions $\mathbf{g}_n(\mathbf{r})$, $n = 1, 2, \ldots, N_{\text{E}}$ [15]. The BC basis functions are dual functions with respect to the RWG basis functions and are defined on barycentrically refined triangular patches. The explicit definition of the BC basis function $\mathbf{g}_n(\mathbf{r})$ is omitted here and can be found in [15]. We denote the Gram matrices associated with the RWG and BC functions as $\mathbf{G}_{\mathbf{f},\mathbf{f}}$ and $\mathbf{G}_{\mathbf{g},\mathbf{g}}$. Their entries are $\{\mathbf{G}_{\mathbf{f},\mathbf{f}}\}_{mn} = \langle \mathbf{f}_m(\mathbf{r}), \mathbf{f}_n(\mathbf{r}) \rangle$ and $\{\mathbf{G}_{\mathbf{g},\mathbf{g}}\}_{mn} = \langle \mathbf{g}_m(\mathbf{r}), \mathbf{g}_n(\mathbf{r}) \rangle$, respectively.

Besides the above-mentioned vector basis functions, used for the discretization of EFIE, scalar basis functions can also be used for the discretization of SIEs. Here, two commonly used sets of scalar basis functions are considered the pyramid basis functions $\lambda_n(\mathbf{r})$, $n = 1, 2, \ldots, N_{\text{V}}$ and their dual functions $\tilde{\lambda}_n(\mathbf{r})$, $n = 1, 2, \ldots, N_{\text{P}}$, where N_{V} and N_{P} denote the number of vertices and triangular patches of the mesh, respectively. The dual-pyramid basis functions $\tilde{\lambda}_n(\mathbf{r})$ are defined on the barycentrically refined triangular patches. The nth pyramid basis function $\lambda_n(\mathbf{r})$ is defined to be equal to 1 at the nth vertex, 0 at the other vertices, and linear on the triangular patches sharing the nth vertex [16]. The explicit definition of $\tilde{\lambda}_n(\mathbf{r})$ is omitted here and can be found in [15]. Similarly, the Gram matrices associated with the pyramid and dual-pyramid functions are $\mathbf{G}_{\lambda,\lambda}$ with dimension $N_{\text{V}} \times N_{\text{V}}$ and $\mathbf{G}_{\tilde{\lambda},\tilde{\lambda}}$ with dimension $N_{\text{P}} \times N_{\text{P}}$, whose entries are $\{\mathbf{G}_{\lambda,\lambda}\}_{mn} = \langle \lambda_m(\mathbf{r}), \lambda_n(\mathbf{r}) \rangle$, and $\{\mathbf{G}_{\tilde{\lambda},\tilde{\lambda}}\}_{mn} = \langle \tilde{\lambda}_m(\mathbf{r}), \tilde{\lambda}_n(\mathbf{r}) \rangle$, respectively.

The Gram matrices introduced above ($\mathbf{G}_{\mathbf{f},\mathbf{f}}$, $\mathbf{G}_{\mathbf{g},\mathbf{g}}$, $\mathbf{G}_{\lambda,\lambda}$, and $\mathbf{G}_{\tilde{\lambda},\tilde{\lambda}}$) are symmetric positive definite (SPD)—since we consider only Gram matrices of bases [4]—and can be used for the normalizations of the EFIE boundary element matrix $\mathbf{T}$, the loop-to-RWG transformation matrix $\mathbf{\Lambda}$, and the star-to-RWG transformation matrix $\mathbf{\Sigma}$, where the explicit definitions of $\mathbf{\Lambda}$ and $\mathbf{\Sigma}$ can be found in [17]. As mentioned in [3], using the matrices multiplied by the inverse square roots of the corresponding Gram matrices $\tilde{\mathbf{T}}$, $\tilde{\mathbf{\Lambda}}$, and $\tilde{\mathbf{\Sigma}}$ instead of their standard counterparts $\mathbf{T}$, $\mathbf{\Lambda}$, and $\mathbf{\Sigma}$ allows for more efficient spectral manipulations for problems involving nonuniformly discretized geometries. These new matrices are obtained by multiplying the standard matrices with the inverse square roots of the corresponding Gram matrices, for example, $\tilde{\mathbf{T}} = \sqrt{\mathbf{G}_{\mathbf{f},\mathbf{f}}}^{-1} \mathbf{T} \sqrt{\mathbf{G}_{\mathbf{f},\mathbf{f}}}^{-1}$. In Section III, strategies for the computation of the square roots and inverse square roots of the real, sparse, and SPD Gram matrices introduced above are presented.

III. Computation of the Square Roots and Inverse Square Roots of the Gram Matrices

To compute the square roots and inverse square roots of the Gram matrices of interest, a simple-to-define but expensive-to-compute approach is leveraging SVD [4]. SVD of a real SPD matrix $\mathbf{G}$ of dimension $N \times N$ is

$$\mathbf{G} = \mathbf{U}\mathbf{S}\mathbf{U}^T \quad (3)$$

where $\mathbf{S}$ is a diagonal matrix with nonzero elements that are the N singular values of $\mathbf{G}$ and $\mathbf{U}$ is a unitary matrix. Here, and in the following, $\mathbf{G}$ stands for any of the matrices $\mathbf{G}_{\mathbf{f},\mathbf{f}}$, $\mathbf{G}_{\mathbf{g},\mathbf{g}}$, $\mathbf{G}_{\lambda,\lambda}$, and $\mathbf{G}_{\tilde{\lambda},\tilde{\lambda}}$. Given that the Gram matrices under consideration are also invertible, their square roots and inverse square roots can be obtained as

$$\sqrt{\mathbf{G}} = \mathbf{U}\bar{\mathbf{S}}\mathbf{U}^T \quad (4)$$

$$\sqrt{\mathbf{G}}^{-1} = \mathbf{U}\bar{\mathbf{S}}^{-1}\mathbf{U}^T \quad (5)$$

where $\bar{\mathbf{S}}$ is a diagonal matrix of which the diagonal entries are the square roots of that of $\mathbf{S}$. However, because of the computational cost of the SVD algorithm, this method quickly becomes impractical for large problems. Note that, since the matrices under consideration are SPD, their respective square roots are unique [18].

In this work, the square roots and inverse square roots of the Gram matrices are expressed as

$$\sqrt{\mathbf{G}} = \sqrt{\|\mathbf{G}\|_2}\, \sqrt{\mathbf{G}/\|\mathbf{G}\|_2} \quad (6)$$

$$\sqrt{\mathbf{G}}^{-1} = \sqrt{\|\mathbf{G}\|_2}^{-1}\, \sqrt{\mathbf{G}/\|\mathbf{G}\|_2}^{-1} \quad (7)$$

where $\|\mathbf{G}\|_2$ denotes the L_2-norm of $\mathbf{G}$. Even though this normalization by $\|\mathbf{G}\|_2$ is not a necessary step of our proposed techniques, it is helpful for our analysis and the value of $\|\mathbf{G}\|_2$ can be computed fast using power methods [19] for sparse, SPD, and well-conditioned matrices. Then, because the Gram matrices under consideration are sparse, $\sqrt{\mathbf{G}/\|\mathbf{G}\|_2}$ and $\sqrt{\mathbf{G}/\|\mathbf{G}\|_2}^{-1}$ are numerically approximated using polynomial expansions-based algorithms combined with the theory of matrix functions [10] as presented in Sections III-A–III-C. Finally, $\sqrt{\mathbf{G}}$ and $\sqrt{\mathbf{G}}^{-1}$ are computed by multiplying $\sqrt{\|\mathbf{G}\|_2}$ and $\sqrt{\|\mathbf{G}\|_2}^{-1}$ with the numerical approximations of $\sqrt{\mathbf{G}/\|\mathbf{G}\|_2}$ and $\sqrt{\mathbf{G}/\|\mathbf{G}\|_2}^{-1}$, respectively. This approach is made possible by the fact

that all the Gram matrices under consideration are sparse, meaning that they can be computed, stored, and multiplied to a vector in linear complexity, which is crucial to maintain compatibility with fast solvers for the overall electromagnetic problem.

To condense the treatments, given a real, sparse, and SPD matrix $\mathbf{X}$ of dimension $N \times N$, we denote $f(\mathbf{X})$ as a matrix function that corresponds to either $\mathbf{X} \mapsto \sqrt{\mathbf{X}}$ or $\mathbf{X} \mapsto \sqrt{\mathbf{X}}^{-1}$. The numerical expression of $f(\mathbf{X})$ can be obtained by generalizing the numerical (polynomial or rational) approximation of its scalar function counterpart $f(x)$, which corresponds to either $x \mapsto \sqrt{x}$ or $x \mapsto \sqrt{x}^{-1}$, $x \in \mathbb{R}^+$, to matrix arguments [10]. Then, the numerical approximations of $\sqrt{\mathbf{G}/\|\mathbf{G}\|_2}$ and $\sqrt{\mathbf{G}/\|\mathbf{G}\|_2}^{-1}$ are obtained by using the expansions of $\sqrt{\mathbf{X}}$ and $\sqrt{\mathbf{X}}^{-1}$ with $\mathbf{X} = \mathbf{G}/\|\mathbf{G}\|_2$. We denote by δ the relative error between $f(\mathbf{X})$—computed, for instance, by SVD—and its approximation $f^{\text{num}}(\mathbf{X})$: $\delta = \|f(\mathbf{X}) - f^{\text{num}}(\mathbf{X})\|_2 / \|f(\mathbf{X})\|_2$.

A. Taylor Series Expansion

As the first algorithmic approach, the Taylor series expansion (TSE) [20] is used for the polynomial approximations of $x \mapsto \sqrt{x}$ and $x \mapsto \sqrt{x}^{-1}$. Using TSEs, $x \mapsto \sqrt{x}$ and $x \mapsto \sqrt{x}^{-1}$ can be numerically expanded around $x = 1$ as

$$x \mapsto \sqrt{x} \approx \sum_{n=0}^{N_\text{T}} c_n^{\text{TSE}} (x-1)^n, \quad \text{and}$$
$$x \mapsto \sqrt{x}^{-1} \approx \sum_{n=0}^{N_\text{T}} \tilde{c}_n^{\text{TSE}} (x-1)^n. \tag{8}$$

Here, N_T is the order of the TSE, and c_n^{TSE} and $\tilde{c}_n^{\text{TSE}}$ are the nth expansion coefficients of TSE for the approximations of $\sqrt{x}$ and $\sqrt{x}^{-1}$, respectively. These coefficients can be computed as

$$c_n^{\text{TSE}} = \frac{\sqrt{x}^{(n)}|_{x=1}}{n!}, \quad \text{and } \tilde{c}_n^{\text{TSE}} = \frac{(1/\sqrt{x})^{(n)}|_{x=1}}{n!}. \tag{9}$$

The approximations of their matrix function counterparts $\mathbf{X} \mapsto \sqrt{\mathbf{X}}$ and $\mathbf{X} \mapsto \sqrt{\mathbf{X}}^{-1}$ are obtained by generalizing (8) to $\mathbf{X}$ as

$$\mathbf{X} \mapsto \sqrt{\mathbf{X}} \approx \sum_{n=0}^{N_\text{T}} c_n^{\text{TSE}} (\mathbf{X}-\mathbf{I})^n, \quad \mathbf{X} \mapsto \sqrt{\mathbf{X}}^{-1} \approx \sum_{n=0}^{N_\text{T}} \tilde{c}_n^{\text{TSE}} (\mathbf{X}-\mathbf{I})^n \tag{10}$$

where $\mathbf{I}$ is the identity matrix with the same dimension as $\mathbf{X}$.

The values of the first ten expansion coefficients of the TSEs $\{c_n^{\text{TSE}}\}_{n=0}^9$ and $\{\tilde{c}_n^{\text{TSE}}\}_{n=0}^9$ are $\{1, (1/2), -(1/8), (1/16), -(5/128), (7/256), -(21/1024), (33/2048), -(429/32\,768), (715/65\,536)\}$ and $\{1, -(1/2), (3/8), -(5/16), (35/128), -(63/256), (231/1024), -(429/2048), (6435/32\,768)$, and $-(12\,155/65\,536)\}$, respectively.

B. Chebyshev Polynomial Expansion

As the second algorithmic approach, the truncated Chebyshev polynomial series expansion (CPE) [21] is used for the polynomial approximations of the square root function and its reciprocal on the interval $x \in [n_0, 1]$ as

$$x \mapsto \sqrt{x} \approx {\sum_{n=0}^{N_\text{C}}}' c_n^{\text{CPE}} T_n(x), \quad \text{and } x \mapsto \sqrt{x}^{-1} \approx {\sum_{n=0}^{N_\text{C}}}' \tilde{c}_n^{\text{CPE}} T_n(x). \tag{11}$$

Here, the primed summation indicates that the first term is halved, n_0 is a positive real number, N_C is the expansion order of CPE, $T_n(x)$ is the shifted Chebyshev polynomial of the first kind of order n defined on the interval $x \in [n_0, 1]$ as

$$T_n(x) = \begin{cases} 1, & \text{if } n = 0 \\ \dfrac{2x - (n_0+1)}{1-n_0}, & \text{if } n = 1 \\ 2\left(\dfrac{2x-(n_0+1)}{1-n_0}\right) T_{n-1}(x) - T_{n-2}(x), & \text{otherwise} \end{cases} \tag{12}$$

and the Chebyshev series coefficients c_n^{CPE} and $\tilde{c}_n^{\text{CPE}}$ for the approximations of $\sqrt{x}$ and $\sqrt{x}^{-1}$ can be computed as [21]

$$c_n^{\text{CPE}} = \frac{2}{\pi} \int_{n_0}^1 \frac{\sqrt{x} T_n(x)}{\sqrt{-x^2 + (n_0+1)x - n_0}} \mathrm{d}x \tag{13}$$
$$\tilde{c}_n^{\text{CPE}} = \frac{2}{\pi} \int_{n_0}^1 \frac{\sqrt{x}^{-1} T_n(x)}{\sqrt{-x^2 + (n_0+1)x - n_0}} \mathrm{d}x \tag{14}$$

which can be rewritten with special functions as

$$c_n^{\text{CPE}} = 2\sqrt{n_0} \frac{{}_3F_2\left(\begin{matrix} -1/2 & 1/2 & 1 \\ 1-n & 1+n \end{matrix}; 1 - n_0^{-1}\right)}{\Gamma(1-n)\Gamma(1+n)} \tag{15}$$
$$\tilde{c}_n^{\text{CPE}} = \frac{2}{\sqrt{n_0}} \frac{{}_3F_2\left(\begin{matrix} 1/2 & 1/2 & 1 \\ 1-n & 1+n \end{matrix}; 1 - n_0^{-1}\right)}{\Gamma(1-n)\Gamma(1+n)} \tag{16}$$

where ${}_3F_2$ is the generalized hypergeometric function [22] and Γ is the Euler gamma function.

Similarly, after the series expansions of $x \mapsto \sqrt{x}$ and $x \mapsto \sqrt{x}^{-1}$ in (11) are derived, their matrix function counterparts can be obtained by generalizing (11) to the matrix arguments as

$$\mathbf{X} \mapsto \sqrt{\mathbf{X}} \approx {\sum_{n=0}^{N_\text{C}}}' c_n^{\text{CPE}} T_n(\mathbf{X}) \quad \mathbf{X} \mapsto \sqrt{\mathbf{X}}^{-1} \approx {\sum_{n=0}^{N_\text{C}}}' \tilde{c}_n^{\text{CPE}} T_n(\mathbf{X}), \tag{17}$$

where direct evaluation of the sum in (17) is not necessarily optimal and other algorithms can be employed [23], and $T_n(\mathbf{X})$ is defined as

$$T_n(\mathbf{X}) = \begin{cases} \mathbf{I}, & \text{if } n = 0 \\ \dfrac{2\mathbf{X} - (n_0+1)\mathbf{I}}{1-n_0}, & \text{if } n = 1 \\ \dfrac{2[2\mathbf{X} - (n_0+1)\mathbf{I}]}{1-n_0} T_{n-1}(\mathbf{X}) - T_{n-2}(\mathbf{X}), & \text{otherwise.} \end{cases} \tag{18}$$

Note that, due to the normalization and the properties of the Gram matrices we study, the spectrum of $\mathbf{X}$—to which the polynomial approximations are applied—lives in the interval $[n_0, 1]$, where n_0 is the inverse of the condition number of $\mathbf{X}$. When using (17), the coefficients c_n^{CPE} and $\tilde{c}_n^{\text{CPE}}$ must be computed for each matrix since they depend on the condition number of the matrix argument n_0^{-1}. If this turns out to be inconvenient, tabulated values of coefficients can be used for the matrices that have a value of n_0 living in known ranges. Usage of such tabulated values will typically yield higher errors than the computation with the matrix-dependent coefficients. In Section IV, we will provide numerical results for these two approaches designated as "CPE-1" for the matrix-specific approach and "CPE-2" for the tabulated approach, respectively. For convenience, the values of c_n^{CPE} and $\tilde{c}_n^{\text{CPE}}$ of CPE-2 are provided in Tables I and II for given bounds on the matrices conditioning (different n_0).

C. Padé Approximant Expansion

The last algorithmic approach we explore is the Padé approximant expansion (PAE) [24] for $x \mapsto \sqrt{x}$ and $x \mapsto \sqrt{x}^{-1}$ at $x = 1$ as

$$x \mapsto \sqrt{x} \approx \frac{\sum_{n=0}^{N_\text{A}} c_n^{\text{PAE}} x^n}{\sum_{n=0}^{N_\text{A}} c_n^{\text{PAE}} x^{N_\text{A}-n}}$$
$$x \mapsto \sqrt{x}^{-1} \approx \frac{\sum_{n=0}^{N_\text{A}} c_n^{\text{PAE}} x^{N_\text{A}-n}}{\sum_{n=0}^{N_\text{A}} c_n^{\text{PAE}} x^n}. \tag{19}$$

Here, N_A is the expansion order of PAE, and c_n^{PAE} is the nth expansion coefficient of PAE for the approximations of $\sqrt{x}$ and $\sqrt{x}^{-1}$, which depends on N_A and can be obtained after solving the linear equation systems as presented in [25].

TABLE I

FIRST 20 CHEBYSHEV SERIES COEFFICIENTS FOR THE SQUARE ROOT FUNCTION FOR DIFFERENT n_0

n_0 \ c_n^{CPE}	c_0^{CPE}	c_1^{CPE}	c_2^{CPE}	c_3^{CPE}	c_4^{CPE}	c_5^{CPE}	c_6^{CPE}	c_7^{CPE}	c_8^{CPE}	c_9^{CPE}
	c_{10}^{CPE}	c_{11}^{CPE}	c_{12}^{CPE}	c_{13}^{CPE}	c_{14}^{CPE}	c_{15}^{CPE}	c_{16}^{CPE}	c_{17}^{CPE}	c_{18}^{CPE}	c_{19}^{CPE}
$n_0 \geq 1\times10^{-1}$	$\frac{50720584}{36057897}$	$\frac{58192354}{176379781}$	$-\frac{4460738}{108096729}$	$\frac{599673}{57061255}$	$-\frac{287819}{85384633}$	$\frac{183411}{150871267}$	$-\frac{58340}{123912171}$	$\frac{51981}{271721903}$	$-\frac{7566}{94035965}$	$\frac{2764}{79582277}$
	$-\frac{201}{13137223}$	$\frac{1188}{173409911}$	$-\frac{409}{131560083}$	$\frac{145}{101639721}$	$-\frac{17}{25723455}$	$\frac{55}{178196989}$	$-\frac{15}{103329721}$	$\frac{3}{43668719}$	$-\frac{1}{30591204}$	$\frac{1}{63979016}$
$n_0 \geq 5\times10^{-2}$	$\frac{141760564}{104989387}$	$\frac{35002745}{95238932}$	$-\frac{5385084}{98048633}$	$\frac{375119}{22232916}$	$-\frac{123075}{18770531}$	$\frac{964144}{335715223}$	$-\frac{99240}{73358167}$	$\frac{61845}{92416364}$	$-\frac{49497}{144355439}$	$\frac{43265}{239826181}$
	$-\frac{8116}{83759003}$	$\frac{4645}{87782356}$	$-\frac{4539}{154958201}$	$\frac{2159}{131648930}$	$-\frac{567}{61162961}$	$\frac{708}{133999337}$	$-\frac{225}{74184637}$	$\frac{187}{106738132}$	$-\frac{91}{89427045}$	$\frac{77}{129639190}$
$n_0 \geq 1\times10^{-2}$	$\frac{94293998}{72892523}$	$\frac{11654085}{28548136}$	$-\frac{13024699}{174927782}$	$\frac{1616566}{56730601}$	$-\frac{1147126}{82276417}$	$\frac{761833}{98466580}$	$-\frac{308484}{66539819}$	$\frac{263708}{90144229}$	$-\frac{162889}{85022700}$	$\frac{161374}{125071371}$
	$-\frac{37949}{42730513}$	$\frac{43604}{70096297}$	$-\frac{29207}{66081562}$	$\frac{51537}{162168061}$	$-\frac{25435}{110193549}$	$\frac{11535}{68213866}$	$-\frac{10239}{82034690}$	$\frac{3604}{38866185}$	$-\frac{6215}{89696092}$	$\frac{2753}{52900755}$
$n_0 \geq 5\times10^{-3}$	$\frac{111282682}{86634283}$	$\frac{19778972}{47632141}$	$-\frac{10097893}{128419878}$	$\frac{1613988}{51323195}$	$-\frac{1103585}{68372228}$	$\frac{1156783}{122811139}$	$-\frac{1072665}{180416284}$	$\frac{182246}{46057955}$	$-\frac{335564}{122664125}$	$\frac{102602}{52715219}$
	$-\frac{86227}{60890409}$	$\frac{77118}{73520351}$	$-\frac{61735}{78300108}$	$\frac{43125}{71884333}$	$-\frac{93187}{202045214}$	$\frac{27405}{76607114}$	$-\frac{26887}{96161515}$	$\frac{1853}{8422610}$	$-\frac{19053}{109416983}$	$\frac{2101}{15164315}$
$n_0 \geq 1\times10^{-3}$	$\frac{67448647}{52859297}$	$\frac{18465778}{43750239}$	$-\frac{3199979}{38492102}$	$\frac{3836927}{109928911}$	$-\frac{1863218}{98477081}$	$\frac{1438469}{122838561}$	$-\frac{1071366}{136237541}$	$\frac{1846182}{330775465}$	$-\frac{1551939}{376426982}$	$\frac{400555}{127615892}$
	$-\frac{362239}{148056512}$	$\frac{272353}{140130127}$	$-\frac{353347}{225334648}$	$\frac{98124}{76560973}$	$-\frac{75049}{70863879}$	$\frac{78769}{89167398}$	$-\frac{41954}{56475965}$	$\frac{258049}{410152123}$	$-\frac{33661}{62777131}$	$\frac{177773}{386862333}$

TABLE II

FIRST 20 CHEBYSHEV SERIES COEFFICIENTS FOR THE INVERSE SQUARE ROOT FUNCTION FOR DIFFERENT n_0

n_0 \ $\tilde{c}_n^{\mathrm{CPE}}$	$\tilde{c}_0^{\mathrm{CPE}}$	$\tilde{c}_1^{\mathrm{CPE}}$	$\tilde{c}_2^{\mathrm{CPE}}$	$\tilde{c}_3^{\mathrm{CPE}}$	$\tilde{c}_4^{\mathrm{CPE}}$	$\tilde{c}_5^{\mathrm{CPE}}$	$\tilde{c}_6^{\mathrm{CPE}}$	$\tilde{c}_7^{\mathrm{CPE}}$	$\tilde{c}_8^{\mathrm{CPE}}$	$\tilde{c}_9^{\mathrm{CPE}}$
	$\tilde{c}_{10}^{\mathrm{CPE}}$	$\tilde{c}_{11}^{\mathrm{CPE}}$	$\tilde{c}_{12}^{\mathrm{CPE}}$	$\tilde{c}_{13}^{\mathrm{CPE}}$	$\tilde{c}_{14}^{\mathrm{CPE}}$	$\tilde{c}_{15}^{\mathrm{CPE}}$	$\tilde{c}_{16}^{\mathrm{CPE}}$	$\tilde{c}_{17}^{\mathrm{CPE}}$	$\tilde{c}_{18}^{\mathrm{CPE}}$	$\tilde{c}_{19}^{\mathrm{CPE}}$
$n_0 \geq 1\times10^{-1}$	$\frac{374048017}{113951175}$	$-\frac{88499941}{99875048}$	$\frac{15797788}{45155977}$	$-\frac{20535446}{134671187}$	$\frac{3198561}{45955201}$	$-\frac{1821274}{55810317}$	$\frac{1646349}{105728006}$	$-\frac{656367}{87247730}$	$\frac{187127}{51011883}$	$-\frac{257569}{142972536}$
	$\frac{337750}{379582213}$	$-\frac{17881}{40498318}$	$\frac{23207}{105516984}$	$-\frac{16946}{154174661}$	$\frac{5735}{104114243}$	$-\frac{1684}{60855691}$	$\frac{1403}{100712358}$	$-\frac{640}{91088439}$	$\frac{138}{38877931}$	$-\frac{197}{109695708}$
$n_0 \geq 5\times10^{-2}$	$\frac{249779459}{67453088}$	$-\frac{350792999}{280590374}$	$\frac{132037463}{217146298}$	$-\frac{17309909}{53231083}$	$\frac{24420789}{134319148}$	$-\frac{11726340}{112404257}$	$\frac{9883564}{162320651}$	$-\frac{3377515}{93897642}$	$\frac{1014741}{47325860}$	$-\frac{16780163}{1303748560}$
	$\frac{510107}{65658935}$	$-\frac{491723}{104378654}$	$\frac{360646}{125772587}$	$-\frac{240771}{137509316}$	$\frac{128666}{120011707}$	$-\frac{79363}{120608489}$	$\frac{30997}{76590848}$	$-\frac{26019}{104339573}$	$\frac{15878}{103168691}$	$-\frac{17123}{180008350}$
$n_0 \geq 1\times10^{-2}$	$\frac{237825977}{50542861}$	$-\frac{39264271}{17952244}$	$\frac{195265677}{138817343}$	$-\frac{103416965}{105120298}$	$\frac{12141478}{16961213}$	$-\frac{81979913}{153769588}$	$\frac{100102199}{248249039}$	$-\frac{41303408}{133947555}$	$\frac{47672400}{200509969}$	$-\frac{10291450}{55779169}$
	$\frac{11305153}{78552187}$	$-\frac{9467215}{83975554}$	$\frac{3834427}{43265789}$	$-\frac{7690733}{110058353}$	$\frac{5948375}{107682632}$	$-\frac{3503490}{80051251}$	$\frac{1048651}{30183225}$	$-\frac{6557825}{237360333}$	$\frac{19174519}{871395101}$	$-\frac{999069}{56928095}$
$n_0 \geq 5\times10^{-3}$	$\frac{564146905}{109693414}$	$-\frac{271445188}{103894561}$	$\frac{203729517}{112913626}$	$-\frac{84437949}{62627027}$	$\frac{49111051}{46961990}$	$-\frac{15609456}{18825521}$	$\frac{63222034}{94771407}$	$-\frac{56599573}{104360532}$	$\frac{38412599}{86436742}$	$-\frac{62114496}{169532831}$
	$\frac{75488883}{248678426}$	$-\frac{2511703}{9946203}$	$\frac{16184137}{76778415}$	$-\frac{21196048}{120119399}$	$\frac{17846601}{120516115}$	$-\frac{7550133}{60623138}$	$\frac{11163511}{106379007}$	$-\frac{5209630}{58817269}$	$\frac{7231330}{96584953}$	$-\frac{11584499}{182801188}$
$n_0 \geq 1\times10^{-3}$	$\frac{630048624}{102215551}$	$-\frac{343367843}{94808470}$	$\frac{294957839}{105949003}$	$-\frac{494742647}{216022718}$	$\frac{1224960907}{629659811}$	$-\frac{206423487}{122566312}$	$\frac{180757935}{122418742}$	$-\frac{130317757}{99758659}$	$\frac{119757642}{102912463}$	$-\frac{36868111}{35375072}$
	$\frac{65195223}{69543947}$	$-\frac{95599410}{112964291}$	$\frac{184341026}{240571663}$	$-\frac{55931467}{80408470}$	$\frac{68082220}{107582399}$	$-\frac{70019489}{121380714}$	$\frac{69973473}{132846113}$	$-\frac{35406207}{73506184}$	$\frac{53675438}{121692277}$	$-\frac{34220975}{84624381}$

TABLE III

FIRST 10 PADÉ SERIES COEFFICIENTS FOR DIFFERENT N_{A}

c_n^{CPE} \ N_{A}	0	1	2	3	4	5	6	7	8	9
c_0^{PAE}	1	1	1	1	1	1	1	1	1	1
c_1^{PAE}	—	3	10	21	36	55	78	105	136	171
c_2^{PAE}	—	—	5	35	126	330	715	1365	2380	3876
c_3^{PAE}	—	—	—	7	84	462	1716	5005	12376	27132
c_4^{PAE}	—	—	—	—	9	165	1287	6435	24310	75582
c_5^{PAE}	—	—	—	—	—	11	286	3003	19448	92378
c_6^{PAE}	—	—	—	—	—	—	13	455	6188	50388
c_7^{PAE}	—	—	—	—	—	—	—	15	680	11628
c_8^{PAE}	—	—	—	—	—	—	—	—	17	969
c_9^{PAE}	—	—	—	—	—	—	—	—	—	19

The numerical expressions of their matrix function counterparts are obtained by generalizing (19) to the matrix arguments as

$$\mathbf{X} \mapsto \begin{cases} \sqrt{\mathbf{X}} \approx \left(\sum_{n=0}^{N_{\mathrm{A}}} c_n^{\mathrm{PAE}} \mathbf{X}^{N_{\mathrm{A}}-n}\right)^{-1} \left(\sum_{n=0}^{N_{\mathrm{A}}} c_n^{\mathrm{PAE}} \mathbf{X}^{n}\right) \\ \sqrt{\mathbf{X}}^{-1} \approx \left(\sum_{n=0}^{N_{\mathrm{A}}} c_n^{\mathrm{PAE}} \mathbf{X}^{n}\right)^{-1} \left(\sum_{n=0}^{N_{\mathrm{A}}} c_n^{\mathrm{PAE}} \mathbf{X}^{N_{\mathrm{A}}-n}\right). \end{cases} \tag{20}$$

The detailed values of the expansion coefficients c_n^{PAE} of PAE for $N_{\mathrm{A}} = 0, 1, \ldots, 9$, are provided in Table III.

D. General Comments

Before the presentation of numerical experiments in Section IV, we would like to attract the readers' attention to the following points.

For the reader's convenience, Table IV lists the order N_{T}, N_{C}, and N_{A} at which the Taylor, Chebyshev, and Padé series should be truncated for the numerical expansion of $\sqrt{\mathbf{X}}$ and $\sqrt{\mathbf{X}}^{-1}$ to reach a target relative error δ for $\mathbf{X}$ with different condition number (different n_0); these truncation orders have been obtained through extensive numerical experiments.

IV. NUMERICAL RESULTS

In this section, some numerical experiments are presented to investigate the advantages and disadvantages of TSE, CPE, and PAE for the computation of $\sqrt{\mathbf{G}}$ and $\sqrt{\mathbf{G}}^{-1}$ for $\mathbf{G} \in \{\mathbf{G}_{\mathbf{f},\mathbf{f}}, \mathbf{G}_{\mathbf{g},\mathbf{g}}, \mathbf{G}_{\lambda,\lambda}, \mathbf{G}_{\bar{\lambda},\bar{\lambda}}\}$ with thorough performance analysis and demonstrate the applicability of the proposed techniques to spectral analysis.

A. Accuracy of the Computation of $\sqrt{\mathbf{G}}$ and $\sqrt{\mathbf{G}}^{-1}$

As the first numerical experiment, the accuracy of the computation of $\sqrt{\mathbf{G}}$ and $\sqrt{\mathbf{G}}^{-1}$ using the proposed techniques is investigated. A PEC sphere of radius 0.5 m centered at the origin and residing in free space is considered. The sphere surface is nonuniformly discretized into three meshes designated as "mesh-1," "mesh-2," and "mesh-3" with $\{N_{\mathrm{E}}, N_{\mathrm{P}}, N_{\mathrm{V}}\} = \{1230, 820, 412\}$, $\{N_{\mathrm{E}}, N_{\mathrm{P}}, N_{\mathrm{V}}\} = \{2193, 1462, 733\}$, and $\{N_{\mathrm{E}}, N_{\mathrm{P}}, N_{\mathrm{V}}\} = \{4449, 2966, 1485\}$, respectively. These sets of meshes are selected so that the resulting Gram matrices are increasingly ill-conditioned for mesh-1, -2,

TABLE IV

TRUNCATION ORDER N_T, N_C, AND N_A FOR THE EXPANSION OF $\sqrt{\mathbf{X}}$ (LEFT) AND $\sqrt{\mathbf{X}}^{-1}$ (RIGHT) TO REACH TARGET δ FOR X WITH DIFFERENT n_0

n_0 \ δ		10^{-2}	10^{-3}	10^{-4}	10^{-5}	10^{-6}
$n_0 \geq 1 \times 10^{-1}$	N_T	12	25	41	59	—
	N_C	3	5	8	11	14
	N_A	3	5	7	8	10
$n_0 \geq 5 \times 10^{-2}$	N_T	21	47	—	—	—
	N_C	4	7	11	15	19
	N_A	4	7	9	12	14
$n_0 \geq 1 \times 10^{-2}$	N_T	—	—	—	—	—
	N_C	6	13	21	31	40
	N_A	8	13	19	—	—
$n_0 \geq 5 \times 10^{-3}$	N_T	—	—	—	—	—
	N_C	8	17	29	41	—
	N_A	10	18	—	—	—
$n_0 \geq 1 \times 10^{-3}$	N_T	—	—	—	—	—
	N_C	12	30	—	—	—
	N_A	16	—	—	—	—

n_0 \ δ		10^{-2}	10^{-3}	10^{-4}	10^{-5}	10^{-6}
$n_0 \geq 1 \times 10^{-1}$	N_T	31	51	72	—	—
	N_C	5	9	12	15	19
	N_A	4	6	8	9	11
$n_0 \geq 5 \times 10^{-2}$	N_T	64	—	—	—	—
	N_C	8	13	17	22	27
	N_A	6	8	11	13	16
$n_0 \geq 1 \times 10^{-2}$	N_T	—	—	—	—	—
	N_C	18	28	39	—	—
	N_A	13	19	—	—	—
$n_0 \geq 5 \times 10^{-3}$	N_T	—	—	—	—	—
	N_C	25	40	—	—	—
	N_A	19	—	—	—	—
$n_0 \geq 1 \times 10^{-3}$	N_T	—	—	—	—	—
	N_C	—	—	—	—	—
	N_A	—	—	—	—	—

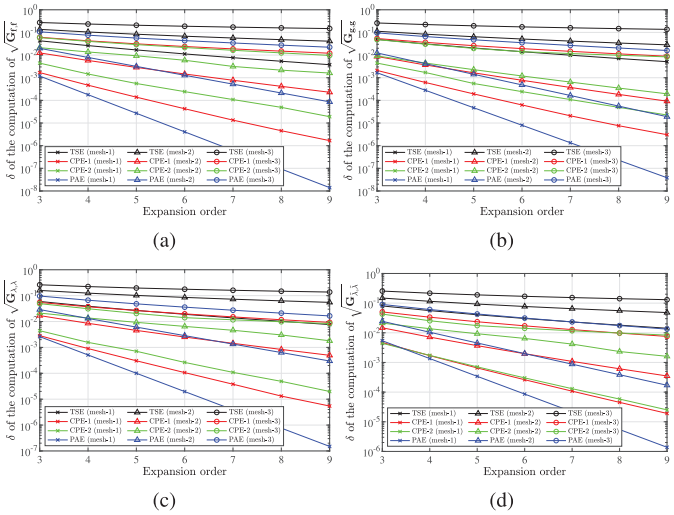

Fig. 1. Relative error δ of the computation of (a) $\sqrt{\mathbf{G}_{\mathbf{f},\mathbf{f}}}$, (b) $\sqrt{\mathbf{G}_{\mathbf{g},\mathbf{g}}}$, (c) $\sqrt{\mathbf{G}_{\lambda,\lambda}}$, and (d) $\sqrt{\mathbf{G}_{\bar{\lambda},\bar{\lambda}}}$ using TSE, CPE-1, CPE-2, and PAE for three mesh sets against the expansion order.

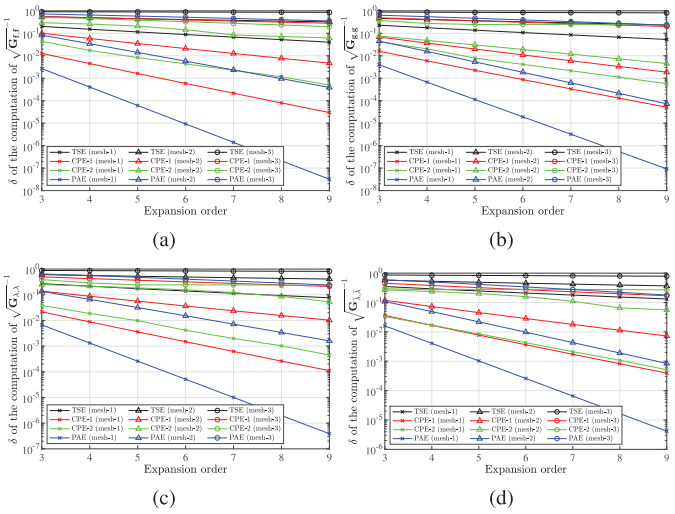

Fig. 2. Relative error δ of the computation of (a) $\sqrt{\mathbf{G}_{\mathbf{f},\mathbf{f}}}^{-1}$, (b) $\sqrt{\mathbf{G}_{\mathbf{g},\mathbf{g}}}^{-1}$, (c) $\sqrt{\mathbf{G}_{\lambda,\lambda}}^{-1}$, and (d) $\sqrt{\mathbf{G}_{\bar{\lambda},\bar{\lambda}}}^{-1}$ using TSE, CPE-1, CPE-2, and PAE for three mesh sets against the expansion order.

and -3 with the condition number of $\{\mathbf{G}_{\mathbf{f},\mathbf{f}}, \mathbf{G}_{\mathbf{g},\mathbf{g}}, \mathbf{G}_{\lambda,\lambda}, \mathbf{G}_{\bar{\lambda},\bar{\lambda}}\}$ equal to $\{5.16, 5.74, 6.72, 9.11\}$, $\{20.45, 14.49, 29.12, 24.58\}$, and $\{615.61, 344.95, 361.91, 269.31\}$, respectively.

Figs. 1(a)–(d) and 2(a)–(d) show the relative error δ of the computation of $\sqrt{\mathbf{G}_{\mathbf{f},\mathbf{f}}}$, $\sqrt{\mathbf{G}_{\mathbf{g},\mathbf{g}}}$, $\sqrt{\mathbf{G}_{\lambda,\lambda}}$, $\sqrt{\mathbf{G}_{\bar{\lambda},\bar{\lambda}}}$ and $\sqrt{\mathbf{G}_{\mathbf{f},\mathbf{f}}}^{-1}$, $\sqrt{\mathbf{G}_{\mathbf{g},\mathbf{g}}}^{-1}$, $\sqrt{\mathbf{G}_{\lambda,\lambda}}^{-1}$, $\sqrt{\mathbf{G}_{\bar{\lambda},\bar{\lambda}}}^{-1}$ for three sets of meshes against the expansion order, respectively, where δ is the relative error between $\sqrt{\mathbf{G}}$ or $\sqrt{\mathbf{G}}^{-1}$ computed using SVD and its numerical computation as described in Section III. As expected, the accuracy of the computation of $\sqrt{\mathbf{G}}$ and $\sqrt{\mathbf{G}}^{-1}$ using the proposed techniques for all the sets of meshes increases with the expansion order. Moreover, for a fixed expansion order and a given algorithm, the accuracy of the numerical computation of $\sqrt{\mathbf{G}}$ and $\sqrt{\mathbf{G}}^{-1}$ improves with mesh uniformity. This is because, as the mesh quality improves, $\mathbf{G}$ exhibits a lower condition number approaching 1 and the numerical computation of $\sqrt{\mathbf{G}}$ and $\sqrt{\mathbf{G}}^{-1}$ improves too (see Section III-D).

Moreover, for mesh-1 (resulting in a lower condition number for $\mathbf{G}$), the PAE converges faster than the TSE and the CPE. In this case, one could choose the PAE that needs fewer expansion orders for a given computational accuracy.

In addition, the figures show that we could use CPE-2 as a good approximation of CPE-1 by directly using the bounds of the known ranges in which n_0 lives and the corresponding coefficients in Tables I and II for CPE for convenience. As one would expect, the error behavior of CPE-1 and CPE-2 converges toward one another when the actual value of n_0 for a given set of meshes and a given Gram matrix corresponds to the lower bound of the range of n_0 (used to select the CPE-2 tabulated coefficients). Additionally, the Chebyshev series truncation order N_C of CPE-2 for the computation of $\sqrt{\mathbf{G}}$ and $\sqrt{\mathbf{G}}^{-1}$ to reach target δ for $\mathbf{G}$ with different condition number in Figs. 1(a)–(d) and 2(a)–(d) generally matches with that reported in Table IV. Also, the accuracy of the computation of $\sqrt{\mathbf{G}}^{-1}$ is generally lower than that of $\sqrt{\mathbf{G}}$ using the same expansion order, the same algorithm, and the same set of meshes for the same $\mathbf{G}$ in Figs. 1(a)–(d) and 2(a)–(d), which is in accordance with the reports in Table IV.

B. Application to Spectral Analysis

As the second numerical experiment, the use of the proposed techniques as a tool for the study, manipulation, and accurate recovery

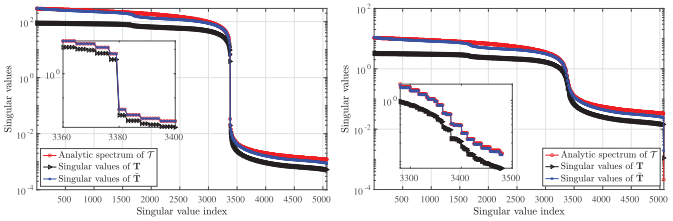

(a) (b)

Fig. 3. Comparison of the singular values of $\mathbf{T}$ and $\tilde{\mathbf{T}}$ with the spectrum of $\mathcal{T}$ including a zoom around singular value index for 3380 (a) $k = 0.1$ rad/m and (b) $k = 2.744$ rad/m.

of the spectrum of the relevant integral operators is showcased. The surface of a PEC sphere of radius 1 m is uniformly discretized with $\{N_E, N_P, N_V\} = \{5070, 3380, 1692\}$ and the corresponding boundary element matrix $\mathbf{T}$ is obtained as delineated in Section II. The spectral analysis is demonstrated for a spurious resonance of the EFIE operator and a nonresonant wavenumber.

Fig. 3(a) and (b) compares the singular values of the standard EFIE matrix $\mathbf{T}$ and its normalized counterpart $\tilde{\mathbf{T}}$ with the analytic spectrum of the surface integral operator $\mathcal{T}$ obtained from a spherical harmonics analysis of the problem [17]. The nonresonant and resonant wavenumbers [26] are, respectively, $k = 0.1$ rad/m and $k = 2.744$ rad/m and the condition numbers of the corresponding $\mathbf{T}$ matrices are 1.7×10^5 and 2.9×10^3. The results are obtained with the PAE for $\sqrt{\mathbf{G}_{\mathbf{f},\mathbf{f}}}^{-1}$ with $N_A = 9$. Clearly, the singular values of $\tilde{\mathbf{T}}$ have a good agreement with the spectrum of $\mathcal{T}$ while those of $\mathbf{T}$ do not, even for the resonant scenario.

When assessing the quality of the spectrum obtained from the BEM matrices of the EM operators, one should keep in mind that several sources of errors will cause deviation of the matrix spectrum from the continuous operator's spectrum. They include the error in the computation of the elements of the BEM matrices—for instance, in the computation of nearly singular integrals [27]—the error caused by the truncation of the expansions of the reciprocal square roots of the Gram matrices, and the error introduced by the spectral properties of the discretization bases [28]. In Fig. 3, these errors degrade the precision of the singular values associated with highly oscillating singular vectors while the rest of the spectrum shows a good agreement with spherical harmonics.

V. Conclusion

In this work, three polynomial-expansion-based algorithms are delineated for the computation of the square roots and inverse square roots of some of the most relevant Gram matrices for SIEs. Properly chosen polynomial expansions of the square root and inverse square root of the scalar functions and the theory of matrix functions are used. Tables containing the different sets of expansion coefficients are provided along with the comparative numerical experiments that illustrate the advantages and disadvantages of the different strategies. Moreover, the application of the proposed techniques to spectral analysis is demonstrated, which could be applied to most of the standard SIEs in electromagnetics and acoustics.

References

[1] J.-M. Jin, *Theory and Computation of Electromagnetic Fields.*, 2nd ed., New York, NY, USA: Wiley, 2015.

[2] D. Boffi, "Compatible discretizations for eigenvalue problems," in *Compatible Spatial Discretizations*, vol. 142. Berlin, Germany: Springer, 2006, pp. 121–142.

[3] A. Merlini, C. Henry, D. Consoli, L. Rahmouni, A. Dély, and F. P. Andriulli, "Laplacian filtered loop-star decompositions and quasi-helmholtz filters: Definitions, analysis, and efficient algorithms," *IEEE Trans. Antennas Propag.*, vol. 71, no. 12, pp. 9289–9302, Dec. 2023.

[4] R. A. Horn and C. R. Johnson, *Matrix Analysis*. Cambridge, U.K.: Cambridge Univ. Press, 2012.

[5] A. F. Peterson, C. F. Smith, and R. Mittra, "Eigenvalues of the moment-method matrix and their effect on the convergence of the conjugate gradient algorithm (EM scattering)," *IEEE Trans. Antennas Propag.*, vol. AP-36, no. 8, pp. 1177–1179, Aug. 1988.

[6] A. Bjorck and S. Hammarling, "A Schur method for the square root of a matrix," *Linear Algebra Appl.*, vols. 52–53, no. 1, pp. 127–140, Jul. 1983.

[7] N. J. Higham, "Newton's method for the matrix square root," *Math. Comput.*, vol. 46, no. 174, p. 537, Apr. 1986.

[8] E. D. Denman and A. N. Beavers, "The matrix sign function and computations in systems," *Appl. Math. Comput.*, vol. 2, no. 1, pp. 63–94, Jan. 1976.

[9] G. W. Stewart, "A Krylov–Schur algorithm for large eigenproblems," *SIAM J. Matrix Anal. Appl.*, vol. 23, no. 3, pp. 601–614, Jan. 2001.

[10] N. J. Higham, *Functions of Matrices: Theory and Computation*. Philadelphia, PA, USA: SIAM, 2008.

[11] Y. Sun, S. Luo, and X. Lei, "Gram matrices of mixed-state ensembles," *Int. J. Theor. Phys.*, vol. 60, no. 9, pp. 3211–3224, Sep. 2021.

[12] R. Chen, A. Merlini, and F. P. Andriulli, "Calculation of inverse square root of RWG Gram matrix based on Chebyshev polynomial expansion," in *Proc. Int. Appl. Comput. Electromagn. Soc. Symp. (ACES-China)*, Xi'an, China, Aug. 2024, pp. 1–2.

[13] S. Rao, D. Wilton, and A. Glisson, "Electromagnetic scattering by surfaces of arbitrary shape," *IEEE Trans. Antennas Propag.*, vol. AP-30, no. 3, pp. 409–418, May 1982.

[14] F. P. Andriulli et al., "A multiplicative Calderon preconditioner for the electric field integral equation," *IEEE Trans. Antennas Propag.*, vol. 56, no. 8, pp. 2398–2412, Aug. 2008.

[15] A. Buffa and S. H. Christiansen, "A dual finite element complex on the barycentric refinement," *Math. Comp.*, vol. 260, no. 6, pp. 1743–1769, 2007.

[16] S. Y. Chen, W. C. Chew, J. M. Song, and J.-S. Zhao, "Analysis of low frequency scattering from penetrable scatterers," *IEEE Trans. Geosci. Remote Sens.*, vol. 39, no. 4, pp. 726–735, Apr. 2001.

[17] S. B. Adrian, A. Dély, D. Consoli, A. Merlini, and F. P. Andriulli, "Electromagnetic integral equations: Insights in conditioning and preconditioning," *IEEE Open J. Antennas Propag.*, vol. 2, pp. 1143–1174, 2021.

[18] C. R. Johnson, K. Okubo, and R. Reams, "Uniqueness of matrix square roots and an application," *Linear Algebra Appl.*, vol. 323, nos. 1–3, pp. 51–60, Jan. 2001.

[19] G. H. Golub and C. F. Van Loan, *Matrix Computations*. Baltimore, MD, USA: The Johns Hopkins Univ. Press, 2013.

[20] B. Taylor, *Methodus Incrementorum Directa Et Inversa*. London, U.K.: Impensis Gulielmi Innys, 1717.

[21] J. C. Mason and C. D. Handscomb, *Chebyshev Polynomials*. London, U.K.: Chapman & Hall, 2002.

[22] F. W. J. Olver, *NIST Handbook of Mathematical Functions*. Cambridge, U.K.: Cambridge Univ. Press, 2010.

[23] C. W. Clenshaw, "A note on the summation of Chebyshev series," *Math. Comput.*, vol. 9, no. 51, pp. 118–120, 1955.

[24] G. A. Baker and P. Graves-Morris, *Padé Approximants*. Cambridge, U.K.: Cambridge Univ. Press, 1996.

[25] Y. Song, N. Sebe, and W. Wang, "Fast differentiable matrix square root and inverse square root," *IEEE Trans. Pattern Anal. Mach. Intell.*, vol. 45, no. 6, pp. 7367–7380, Jun. 2023.

[26] R. F. Harrington, "Spherical wave functions," in *Time-Harmonic Electromagnetic Fields*. Piscataway, NJ, USA: Wiley, 2001, ch. 6, pp. 264–316.

[27] M. M. Botha, "A family of augmented Duffy transformations for near-singularity cancellation quadrature," *IEEE Trans. Antennas Propag.*, vol. 61, no. 6, pp. 3123–3134, Jun. 2013.

[28] K. F. Warnick, *Numerical Analysis for Electromagnetic Integral Equations.* Norwood, MA, USA: Artech House, 2008.